Lawrence Berkeley National Laboratory
LBL Publications

Title
Y-shaped tricatenar azobenzenes – functional liquid crystals with synclinic–anticlinic transitions and spontaneous helix formation

Permalink
https://escholarship.org/uc/item/7tq961sj

Journal
Journal of Materials Chemistry C, 8(37)

ISSN
2050-7526

Authors
Alaasar, Mohamed
Poppe, Silvio
Cao, Yu
et al.

Publication Date
2020-10-01

DOI
10.1039/d0tc03321a

Peer reviewed

eScholarship.org Powered by the California Digital Library
University of California

Y-shaped tricatenar azobenzenes – Functional liquid crystals with synclinic-anticlinic transitions and spontaneous helix formation

Mohamed Alaasar[a,b], Silvio Poppe[a], Yu Cao[c,d], Changlong Chen[c], Feng Liu[c], Chenhui Zhu[d], and Carsten Tschierske[a]

[a] Institute of Chemistry, Martin Luther University Halle-Wittenberg, Kurt Mothes Str. 2, D-06120 Halle (Saale), Germany; carsten.tschierske@chemie.uni-halle.de

[b] Department of Chemistry, Faculty of Science, Cairo University, P.O. 12613 Giza, Egypt; malaasar@sci.cu.edu.eg

[c] State Key Laboratory for Mechanical Behaviour of Materials, Shaanxi International Research Center for Soft Matter, School of Materials Science & Engineering, Xi'an Jiaotong University, Xi'an 710049, P. R. China; feng.liu@xjtu.edu.cn

[d] Advanced Light Source, Lawrence Berkeley National Laboratory, Berkeley, CA 94720, USA: chenhuizhu@lbl.gov

Abstract

A series of achiral tricatenar rod-like molecules with a 3,5-disubstitution pattern at one end and a single alkyl chain at the other end of a rod-like azobenzene derived core is reported. Depending on temperature and alkyl chain length, these Y-shaped compounds self-assemble into different types of liquid crystalline phases, ranging from non-tilted and synclinic tilted hexatic, via non-tilted and anticlinic tilted smectic and bicontinuous cubic LC phases, to a spontaneous mirror symmetry broken isotropic liquid ($Iso_1^{[*]}$) or a related achiral liquid network phase (Iso_1). An additional tilted, but uniaxial smectic phase was observed at the transition between anticlinic and synclinic tilt correlation and was investigated by soft resonant X-ray scattering with respect to possible helix formation. This work provides a new concept for the design of technological interesting azobenzene based LC materials with anticlinic tilted smectic C phases (SmC_a). Moreover, the azobenzene unit is self-assembled in bicontinuous cubic and chiral isotropic liquid phases with long range or short range helical network structures, respectively. Core fluorination removes all lamellar phases, leaving only the cubic phase over wide temperature ranges, even at ambient temperature.

1. Introduction

There are numerous well established and presently developing applications of liquid crystals (LC) in optical displays,[1] organic electronics and photovoltaics,[2,3,4] in selective membranes,[5] for ion conducting arrays[2,5] and in nanoscale patterning on the sub-10 nm length scale for use in nanolithography,[6-8] all being essential for the development of present and future technologies. For LC materials there are three fundamental design concepts, molecular shape, amphiphilicity/polyphilicity[9] and chirality.[10-12] With respect to the molecular shape rod-like and disc-like molecules, leading to lamellar and columnar LCs, respectively, represent the majority.[13] More recently, bent molecules[14,15] and polycatenar molecules, having more than only one flexible chain attached to one or both ends of a rod-like polyaromatic core, have received growing attention (Scheme 1). The latter can show transitions from lamellar (smectic = Sm) via bicontinuous cubic (Cub_{bi}) to columnar (Col) LC phases.[16-20]

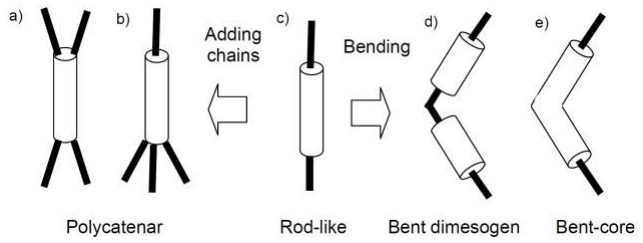

Scheme 1. Different molecular shapes derived from rod-like mesogens by alkyl chain design and by bending the core structure, both leading to mirror symmetry broken mesophases.

In recent years a new feature of polycatenar supramolecular self-assembly was recognized when spontaneous mirror symmetry breaking was observed[9,21-27] due to helix formation by clashing of the peripheral chains which cooperatively couples with chirality synchronization of the involved molecules.[12,22,23] Helical self-assembly has a strong impact on the mesophase structures and leads to complex cubic and non-cubic mesophases with 3D lattices in the case of polycatenars,[28-30] as for example the cubic *I*23 (previously "*Im*3;$^{\bar{}}$*m*")[23,31,32] and the tetragonal SmQ phase.[33-37] Soft helical superstructures can also be found in other classes of mesogenic compounds, like the bent mesogenic dimers and bent-core mesogens (Scheme 1d,e)[12,14,38-59] A local helical organization can even be retained in the isotropic liquid phases of some polycatenars, occurring adjacent to bicontinuous cubic phases.[21] These isotropic liquids spontaneously segregate into a conglomerate of two immiscible chiral fluids with opposite chirality sense ($Iso_1^{[*]}$ phases).[21] This new dynamic mode of chirality synchronization was experimentally observed for different types of achiral, but transiently

chiral tetracatenar molecules (Scheme 1a,b).[21, 60, 61] Photoisomerizable polycatenars with azobenzene units are rare,[62-66] but we succeeded in designing molecular and supramolecular azobenzene based polycatenars forming the symmetry broken isotropic liquid ($Iso_1^{[*]}$).[67,68] In a previous communication we reported that the tricatenar compounds **4-8** with a 3,5-substitution pattern at one end (Scheme 2) can be switched between chiral and achiral states by photo-induced *trans-cis* isomerization.[69]

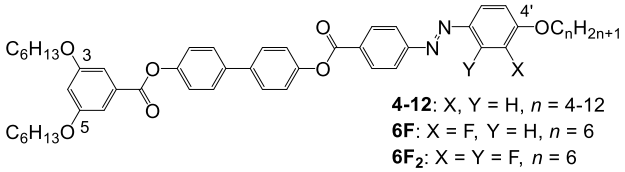

Scheme 2. Tricatenar compounds under investigation; the compound name indicates the number of carbon atoms in the 4'-positioned terminal alkoxy chain.

Herein we expand this work to the full series of compounds **4-12** (Scheme 2) including two core fluorinated derivatives (**6F** and **6F2**) and mainly focus on the series of unusual smectic and hexatic phases formed by these compounds. Special attention is paid to the formation of anticlinic SmC_a phases[70] instead of the synclinic SmC_s phases usually observed for polycatenar compounds[17] and the unexpected transition to synclinic tilted ($HexF_s$, $HexI_s$) and non-tilted (HexB) hexatic phases occurring below them. Not only the inverted temperature dependence of the anticlinic to synclinic transitions is remarkable, even more surprising is, that for one homologue the tilted smectic phase becomes optically uniaxial in a certain temperature range. The possibility of helix formation as origin of optical uniaxiality was investigated by resonant soft X-ray scattering (RSoXS) at the carbon K-edge. In addition, it is shown that formation of mirror-symmetry broken liquids can be tailored by alkyl chain design and that bicontinuous networks with cubic symmetry become dominating after core fluorination.

2. Experimental

Synthesis. **-** The synthesis of the azobenzene-based materials **4-8** has been described in detail previously.[69] The synthesis of the longer homologues **9-12** and the two fluorinated compounds **6F** and **6F2** was carried out in an analogous way (Scheme 3) as reported in the electronic supporting information (ESI).

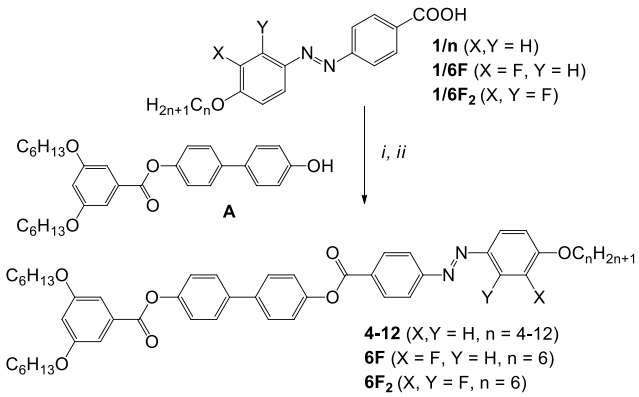

Scheme 3. Synthesis of compounds **4-12**,[69] **6F** and **6F**$_2$. Reagents and conditions: *i*) DMF, $SOCl_2$, reflux 1 hr.; *ii*) dry CH_2Cl_2, dry TEA, dry pyridine, reflux for 6 hr.

Investigations. - The compounds were investigated by polarizing optical microscopy (POM), differential scanning calorimetry (DSC) and X-ray diffraction (XRD) as described in the SI. Resonant RSoXS was performed on BL 11.0.1.2 at the Advanced Light Source in Lawrence Berkeley National Laboratory as described in the SI.

3. Results and Discussion

3.1. Non-fluorinated compounds 4-12

The observed phase sequences and transition temperatures of all investigated compounds are collated in Table 1 and the development of the distinct modes of LC self-assembly in the homologous series of the non-fluorinated compounds **4-12** is shown graphically in Fig. 1. For compounds **5-8** with intermediate chain length a symmetry broken percolated isotropic liquid phase ($Iso_1^{[*]}$, the asterisk in square brackets indicates a conglomerate of enantiomeric liquids) is formed, either above a non-tilted lamellar (SmA) phase (compounds **5**, **6**) or a bicontinuous cubic phase with $Ia3;\bar{}d$ symmetry (compounds **7**, **8**) before the transition to the ordinary achiral liquid takes place.[66] For the longer homologues with n = 9-12 the cubic phase becomes dominating and the symmetry broken chiral conglomerate type $Iso_1^{[*]}$ phase is replaced by an achiral percolated liquid phase (Iso_1). Figure 1 also shows that the SmA phase is replaced by an anticlinic tilted SmC_a phase at lower temperature and that with increasing chain length hexatic LC phases become dominating as low temperature phases below the cubic phase.

Table 1. Phase transition temperatures (*T*/°*C*), mesophase types, and transition enthalpies [Δ*H*/kJ mol^{-1}] of compounds **4-12**, **6F** and **6F$_2$**.

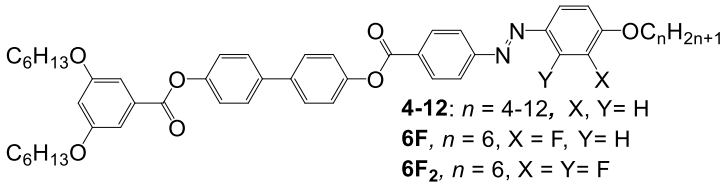

Comp.	*n*	Phase transitions
4	4	*H*: Cr 104 [42.1] SmC_a 178 [-] SmA 201 [2.3] Iso *C*: Iso 199 [-3.4] SmA 177 [-] SmC_a 75 [-34.2] Cr
5	5	*H*: Cr 103 [45.6] SmC_a 168 [-] SmA 180 [1.6] $Iso_1^{[*]}$ 184 [-] Iso *C*: Iso 183 [-] $Iso_1^{[*]}$ 178 [-1.8] SmA 167 [-] SmC_a 65 [-0.2] $HexF_s$ 63 [-0.5] $HexI_s$ 55 [-15.9] Cr
6	6	*H*: Cr 89 [36.5] SmC_a 151 [-] SmA 173 [1.5] $Iso_1^{[*]}$ 184 [-] Iso *C*: Iso 182 [-0.05] $Iso_1^{[*]}$ 171 [-1.6] SmA 150 [-] SmC_a 79 [-]$HexF_s$ 68 [-1.2] $HexI_s$
7	7	*H*: Cr 85 [31.6] SmC_a 134 [1.1] Cub 175 [1.8] $Iso_1^{[*]}$ 185 [-] Iso *C*: Iso 183 [-] $Iso_1^{[*]}$ 132 [-] Cub_{bi}+M 130 [-1.4][b] SmC_a 82 [-] $HexF_s$ 75 [-2.2] HexB 38 [-13.8] Cr
8	8	*H*: Cr 71 [27.6] HexB 87 [2.8] SmC_a 91 [-] SmC_X 94 [-] SmC 124 [1.7] Cub_{bi} 178 [2.7] $Iso_1^{[*]}$ 181 [-] Iso *C*: Iso 181 [-] $Iso_1^{[*]}$ 139 [-0.44] Cub_{bi}+M 106 [-1.6] SmC 94 [-] SmC_X 91 [-] SmC_a 86 [-3.5] HexB
9	9	*H*: Cr 107 [51.2] Cub_{bi} 176 [2.9] Iso *C*: Iso 171 [-0.3] Iso_1 157 [-1.2] Cub_{bi} 75 [-] $HexI_s$ 62 [-7.3] Cr *H2*: $HexI_s$ 91 [-] SmC_a 95 [3.3] Cub_{bi} 176 [2.9] Iso[c]
10	10	*H*: Cr_1 70 [26.9] Cr_2 84 [6.2] Cub_{bi} 171 [2.9] Iso *C*: Iso 167 [-0.5] Iso_1 155 [-1.3] Cub_{bi} 77 [-] $HexI_s$ 47 [-7.3] Cr
12	12	*H*: Cr 100 [35.8] Cub_{bi} 176 [2.9] Iso *C*: Iso 172 [-0.9] Iso_1 158 [-1.3] Cub_{bi} 80 [-] $HexI_s$ 58 [-8.4] Cr
6F	6	*H*: Cr 102 [39.8] Cub_{bi} 168 [2.7] Iso *C*: Iso 138 [-1.1] Cub_{bi} <20 Cr
6F$_2$	6	*H*: Cr 92 [41.7] Cub_{bi} 152 [1.9] Iso *C*: Iso 127 [-1.3] Cub_{bi} <20 Cr

[a] Peak temperatures as determined from 2nd heating (upper lines; *H*) and 2nd cooling DSC scans (lower lines; *C*) with rate 10 K min^{-1}; Abbreviations: Cr = crystalline solid; Iso = isotropic liquid; Iso_1 = achiral cybotactic isotropic liquid; $Iso_1^{[*]}$ spontaneous symmetry broken Iso_1 phase; SmA = nontilted SmA phase; SmC_a = anticlinic tilted smectic C phase; SmC = smectic C phase, having predominating synclinic tilt correlation; SmC_x = optical uniaxial smectic C phase; $HexF_s$ = synclinic tilted hexatic F phases; $HexI_s$ = synclinic tilted hexatic I phases (see Fig. 5i,j); HexB is a non-tilted hexatic B phase (see Fig. 9b); Cub_{bi} = bicontinuous cubic phase with achiral $Ia3;\bar{d}$ lattice; M = birefringent mesophase with non-cubic 3D lattice and unknown structure (see Section 3.2.5). [b]Enthalpy involves both transitions $Iso_1^{[*]}$ - Cub_{bi} and Cub_{bi} - SmC_a.[69] [c] Second heating after cooling to 70 °C; for DSCs, see Fig. S1.

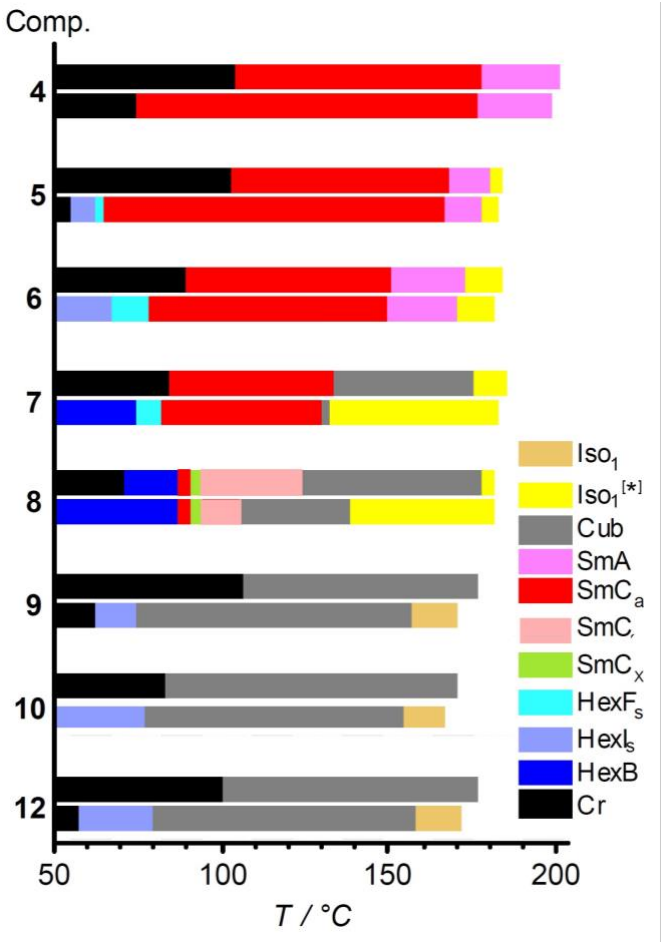

Figure 1. Bar diagram showing the mesophases and phase transitions of compounds **4-12** on heating (upper columns) and on cooling (lower columns); for explanations of the phase types, see footnote in Tab. 1.

3.1.1 Non-tilted SmA and anticlinic tilted SmC_s phases

The smectic high temperature phases of compounds **4-6** show typical fan-like textures with dark extinctions coinciding with the orientations of polarizer and analyzer in planar alignment. In homeotropic alignment they appear optically isotropic in all cases (see Fig. 2a for an example), indicating an SmA phase, where the molecules are organized in layers with the molecular long axes aligned on average parallel to the layer normal. Upon cooling a weakly birefringent Schlieren texture forms in the homeotropic areas whereas the orientation of the dark extinctions in planar samples does not change at this phase transition (Fig. 2b). Moreover, in thin homeotropic samples a stripe pattern is observed (Fig. 2d).[71] This could indicate either a transition to a non-tilted biaxial SmA_b phase by freezing the rotation around the long axis [72 - 76] or an anticlinic tilted SmC_a phase.[70, 77] The slight decrease of the birefringence in the planar texture at the phase transition (colour of the fans changes from yellowish green to green, Fig. 2a→b), indicates the onset of tilt, being in line with the

decrease of the XRD layer spacing at this transition (Fig. 3a). Because the direction of the extinctions in the planar aligned areas remains parallel to the polarizers (Fig. 2a→b→c) the emerging tilt is opposite in adjacent layers, i.e. this is an anticlinic SmC_a phase.[70] This SmA-SmC_a transition takes place without measurable enthalpy change (see DSCs in Fig. S1a,b).
On further cooling the birefringence in the planar aligned area decreases, whereas it increases in the homeotropic (gray) areas, indicating a growing tilt angle in the SmC_a phase range (Fig. 2b→c). For compound **4** with the shortest alkyl chain at the monosubstituted end, this SmC_a phase crystallizes on further cooling, whereas for the following homologues additional phase transitions can be observed, which will be discussed further below.

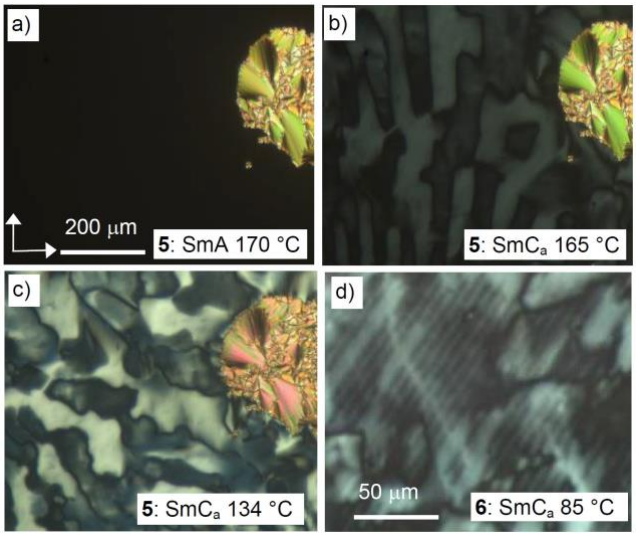

Figure 2. Textures observed between crossed polarizers (white arrows in a) for the SmA-SmC_a transition of a-c) compound **5**, between ordinary microscopy glass plates, showing coexisting homeotropic (dark area) and planar alignment (birefringent area) and d) equidistant stripe patterns observed for compound **6** in the SmC_a phase; for the textures of the HexI phase of **5**, see Fig. S2.

Figure 3 shows the results of XRD studies of compound **6**. The initial increase of the *d*-spacing in the SmA range below 100 °C is in line with a growing packing density with decreasing temperature. The decreasing *d*-value of the XRD layer reflection at this transition (Fig. 3a) confirms the developing tilt at the SmA-SmC_a transition. At the SmA-SmC_a transition temperature the *d*-value (d = 5.22 nm) has a local maximum and is larger than the molecular length in the most extended conformation ($L_{mol,max}$ = 4.5 nm, Fig. 4a). This indicates the formation of an intercalated structure with antiparallel molecular packing and overlapping of the terminal alkyl chain at the monosubstituted end with the aromatics at the opposite ends of the adjacent molecules (Fig. 4b-d). Depending on the degree of intercalation the layer spacing can change from d_{min} = 4.5 nm for the fully intercalated structure (Fig. 4a)

to d_{max} = 5.6 nm for the structure where the two hexyl chains at the 3,5-disubstituted end are completely excluded from intercalation and assume a tuning fork like conformation (Fig. 4c).

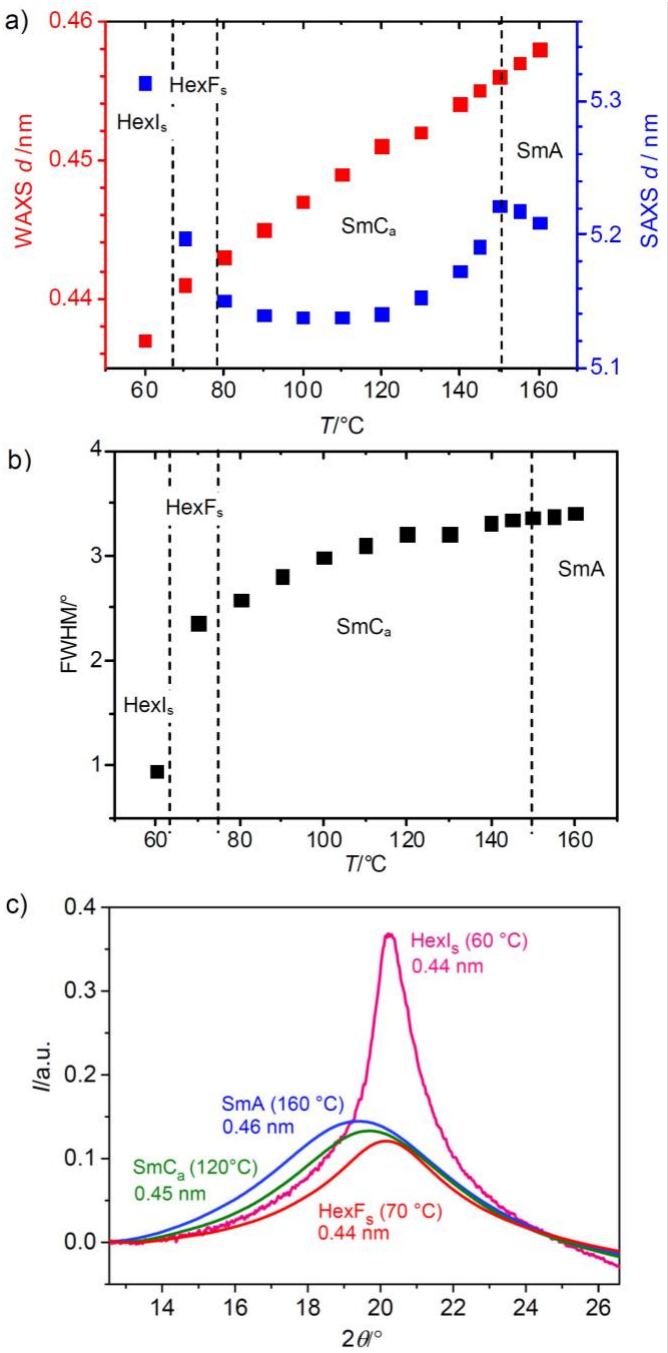

Figure 3. XRD of compound **6** in the different mesophases: a) temperature dependence of the *d*-spacing of the WAXS scattering (red) and the SAXS (10)-reflection (blue); b) FWHM and c) shapes of the WAXS as a function of temperature (with *d*-values of the scattering maxima).

The densest molecular packing would be achieved in the arrangement shown in Fig. 4c, where only the 3,5-chains at the more substituted end are segregated from the residue of the molecule (polyaromatic core + single 4'-alkyl chain). This provides a similar cross sectional area for the two intercalated segments and the two 3,5-hexyl chains, allowing a non-distorted

packing in layers. If the intercalated structure as shown in Fig. 4c is assumed, a maximum tilt β of ~23° is calculated according to $\cos\beta = d/d_{max}$ for the SmC_a phase. It was not possible to determine the actual tilt in the SmC_a phases directly, as the tilt is anticlinic and therefore cannot be observed optically, and in addition, no aligned samples were obtained for XRD investigations. However, an optical tilt of 15° was measured in the synclinic $HexF_s$ phase and 10-11° in the $HexI_s$ phase of compound **6** (Section 3.1.2). Comparing the development of the *d*-values of the layer reflection (Fig. 3a) with these tilt angles leads to an estimated tilt in the range of 15-20° for the SmC_a phase.

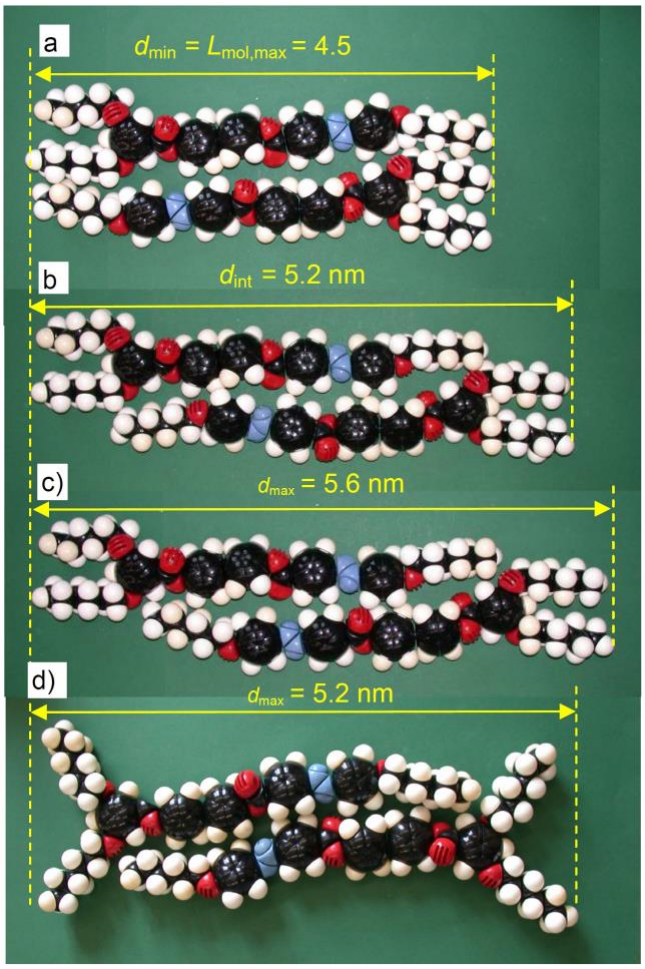

Figure 4. Molecular dimensions of various molecular pairs of compound **6** depending on the degree of intercalation and the *d*-spacing of these possible arrangements within the layers.

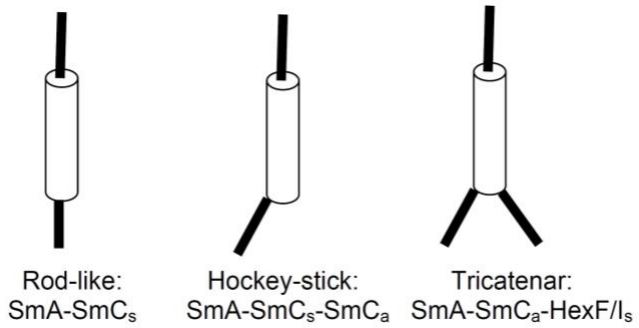

Figure 5. Effect of the chain topology on the phase sequence on cooling.

For achiral rod-like molecules, the synclinic layer correlation is usually favoured by the molecular fluctuations between the layers (out-of-plane fluctuations);[54,78] therefore, the formation of an anticlinic SmC_a phase is surprising. Anticlinic SmC_a phases were first observed for enantiomerically enriched (scalemic) or uniformly chiral rod-like molecules, often with branched (methyl or trifluoromethyl substituted) alkyl side chains.[79] For achiral and racemic molecules it can be promoted by bent spacer units in di- or oligomesogens,[80] especially those with siloxane spacers,[81-84] by mixing rod-like with bent core molecules,[85] by alkyl chain branching (swallow tailed compounds)[86-91] and end group modification,[92,93] including fluorination.[91,94,95,96] However, it was not reported previously for polycatenar (multi-chain rod-like) compound, which form exclusively synclinic SmC_s phases.[17,19,97] However, for the so-called hockey-stick molecules with only two terminal chains, one in the 4-position, and the other one at the opposite end in the 3-position (Fig. 5), the N-SmC_s-SmC_a polymorphism is typically observed on cooling.[98-103] It appears that this 3-substitution provides an increased chain disorder which decouples the layers more efficiently than the chains in 4-position. This suppresses the out of plane fluctuations and therefore favours SmC_a over SmC_s. For the 3,5-disubstitution pattern of the tricatenars this effect is doubled by the two chains in the 3- and in 5-positions, so that only a direct SmA-SmC_a transition without intermediate SmC_s phase is observed for compounds **4-6** (Fig. 5). Thus, the 3,5-disubstitution pattern represents a new powerful design concept for antiferroelectric and eventually orthoconic[104] LC materials. The Y-shaped molecules with 3,5-substitution pattern anyhow resemble Siamese twins of two parallel fused hockey stick molecules (Fig. 5). Simultaneously, they can be considered as a special kind of swallow tailed molecules with the swallow-tail being fused with the rod-like core. Thus, these molecules provide a link between different classes of compounds favoring the anticlinic tilt correlation, namely the swallow-tailed and the bent molecules.

The wide angle scattering (see Fig. 3c) is diffuse in the SmA and SmC_a ranges, being in line with smectic phases with only short-range in-plane order. However, the position of the scattering maximum is continuously shifted from 0.46 nm in the SmA phase to 0.44 nm at the low temperature end of the SmC_a phase (80 °C) (see red dots in Fig. 3a) and the peak width also decreases, in line with a growing packing density (see Fig. 3b,c).

3.1.2 Transition to hexatic phases with synclinic tilt

For compound **4** exclusively the SmA and SmC_a phases were observed whereas for compounds **5-9** additional lamellar phases with enhanced packing density were found below the SmC_a phase (Table 1) as indicated by the changes in the optical textures and XRD patterns.

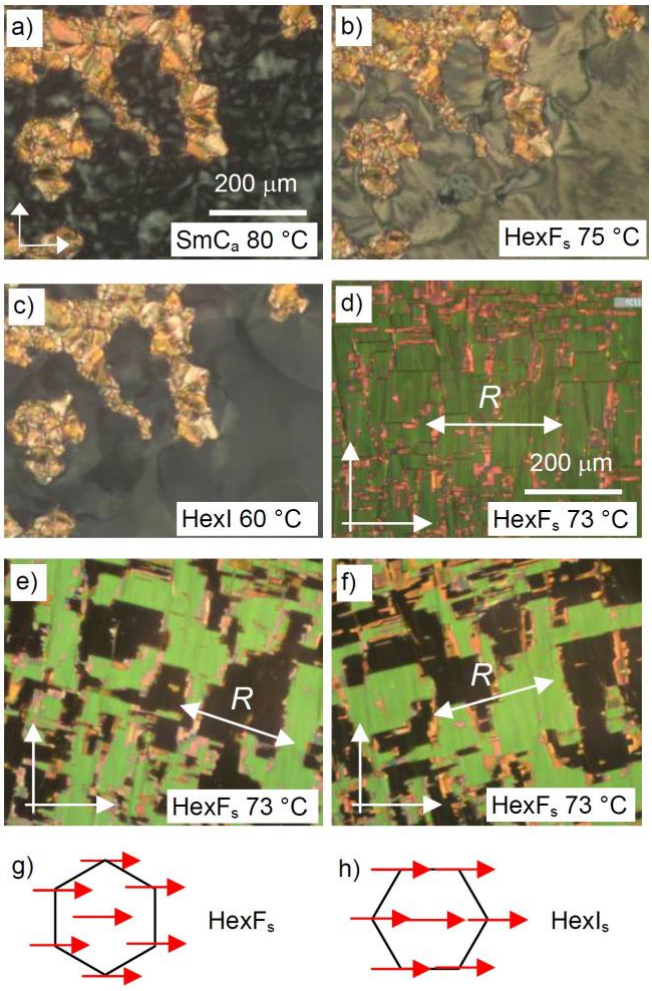

Figure 6. a-c) Phase transitions as observed by polarizing microscopy in the distinct lamellar phases of compound **6** between plain microscopy glass plates on heating; for additional textures, see Fig. S3. d-f) rotating the sample (in planar cell, 6 µm, *R* indicates the rubbing direction) between crossed polarizers indicates a tilt of 15° at T = 73 °C; there is no change of the texture at the transition to $HexI_s$, only the tilt decreases to 10° at T = 60 °C; g,h) show the tilt orientation in the hexatic F and I phases, respectively.

Compounds **5** and **6** behave very similar (for DSCs, see Fig. S1a,b) and Figure 6 shows the change of the textures for compound **6** as a representative example. Upon cooling the SmC_a phase of compound **6** to T = 79 °C the birefringence in the homeotropic areas suddenly increases, accompanied by textural changes in the planar aligned regions; the dark extinctions become birefringent; and the fan texture becomes broken, indicating a change of the tilt from anticlinic to synclinic (Fig. 6a→b). A synclinic tilt of 15° can be determined from the tilt-domain texture by rotation of the sample between the crossed polarizers, as shown in Fig. 6d-f. In the XRD pattern the small angle scattering is shifted at the transition at 79 °C to a bit larger *d*–values and there is a slight reduction of the FWHM of the WAXS (Fig. 3). These are typical features for a SmC_a-$HexF_s$ transition.[105]

At the next transition at 68 °C the homeotropic Schlieren textures become mosaic-like which indicates a transition to another synclinic tilted lamellar phase. The birefringence of the homeotropic aligned areas decreases (Fig. 6c), in line with a decreasing tilt to 10° observed in the corresponding planar tilt-domain texture. The shape of the wide angle scattering becomes much narrower with a slightly non-symmetric lambda–shape as typical for a $HexI_s$ phase (Fig. 3c, magenta curve).[106-110] Thus, the phase sequence SmC_a-$HexF_s$-$HexI_s$ is proposed for compounds **5** and **6**. In the hexatic phases a pseudo-hexagonal packing of the molecules takes place. However, the 2d lattices in adjacent layers are not long range and positionally uncorrelated, leading to only bond orientational order instead of long range periodicity (see Fig. 6h).[107-116] The direction of the tilt with respect to the pseudo-hexagonal lattice distinguishes the hexatic F and I phases (Fig. 6g,h). The increase of the *d*-spacing by ~0.15 nm at the transition from SmC_a via $HexF_s$ to $HexI_s$ (Fig. 3a) can partly be attributed to the growing packing density, causing an alkyl chain stretching and partly to a decreasing tilt with lowering temperature as typical feature of SmC-HexF-HexI transitions.[111] Here, the smectic-to-hexatic transition is associated with the transition from anticlinic to synclinic tilt.[79,113]

3.1.3 Transition from synclinic tilted to non-tilted hexatic phases of compounds 7 and 8

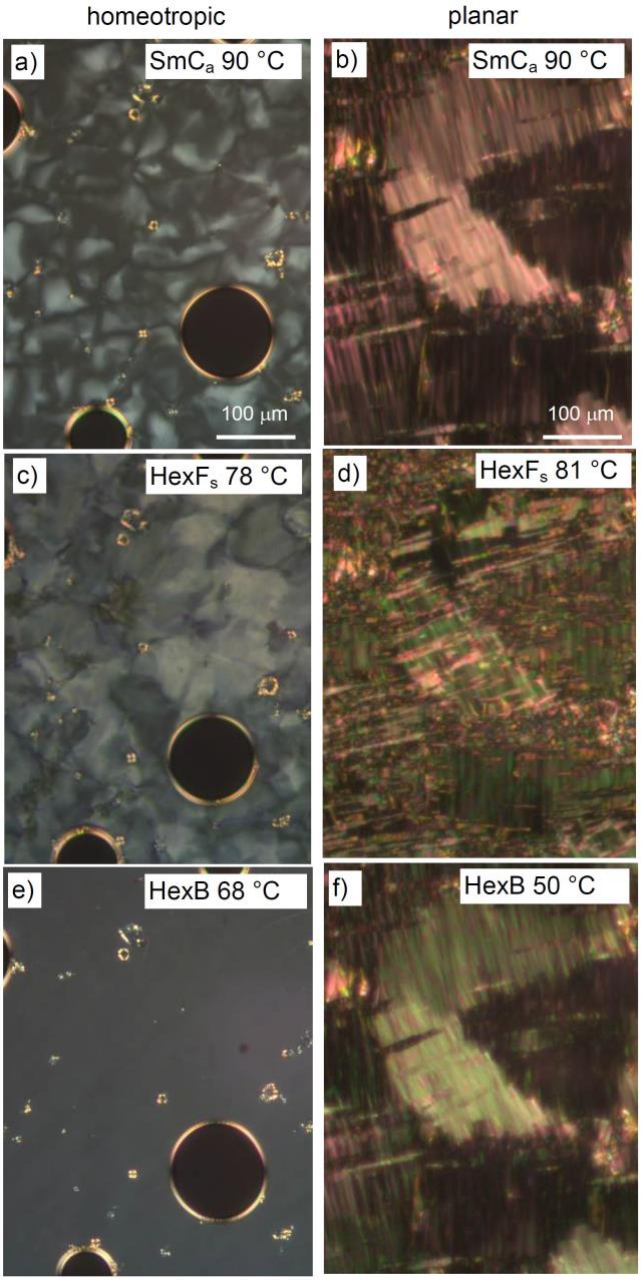

Figure 7. Textures observed for the distinct smectic phases of compound **7** in homeotropic (left) and a planar alignment (right) at the indicated temperatures; the textures at the left were observed between plain microscopy glass plates, whereas those right were recorded in a 6 μm PI-coated ITO cell; in planar alignment the birefringence grows with lowering temperature.

For compounds **7** and **8** the SmA phase is replaced by a cubic phase, whereas the tilted lamellar phases are retained.[117] Upon cooling, the SmC_a phase of compound **7** converts at 82-83 °C into the synclinic $HexF_s$ phase (see Fig. 7b→d). On further cooling to 75 °C the dark extinctions parallel to the polarizers reappear again in the planar samples (Fig. 7d→f) and the homeotropic areas become optically isotropic (Fig. 7c→e) indicating the transition to an optically uniaxial lamellar phase. At this temperature the profile of the XRD wide angle

scattering becomes narrower (magenta curve in Fig. 8c) as typical for a transition to a HexB phase. This means that in this case the tilt is not only reduced, but apparently completely removed at the transition to the low temperature hexatic (HexB) phase.

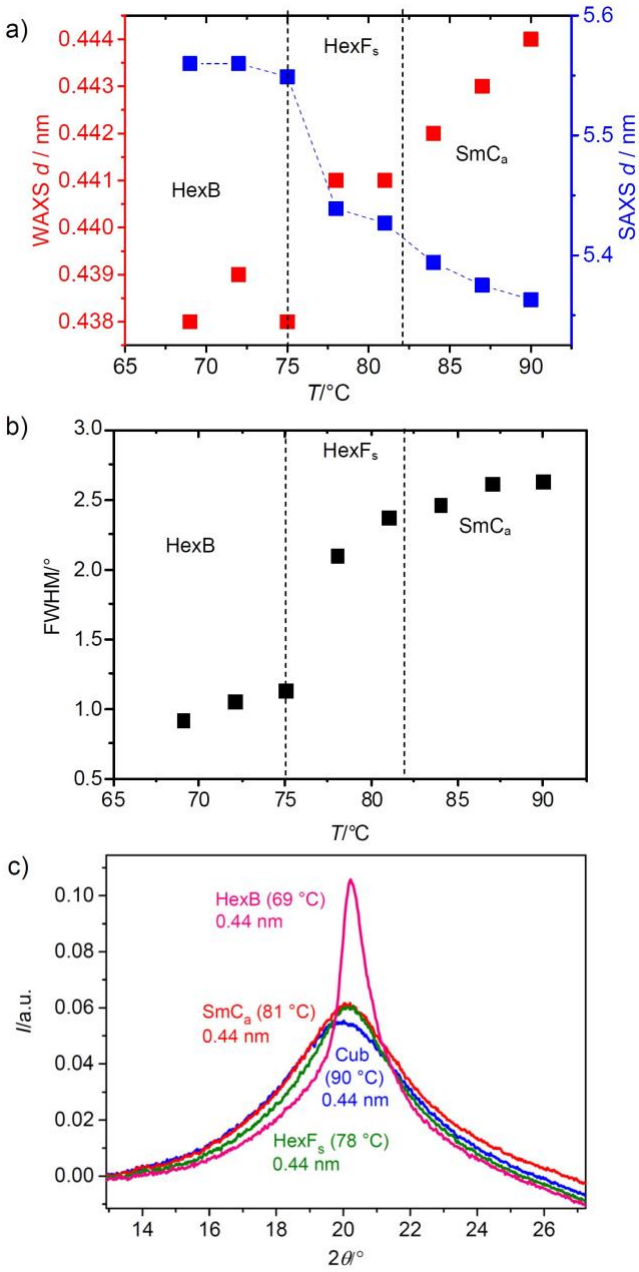

Figure 8. XRD of compound **7** in the different mesophases: a) temperature dependence of the *d*-spacing of the SAXS reflections and the WAXS maximum; b) FWHM and c) line-shape of the WAXS as a function of temperature with *d*-values of the scattering maxima (see also Fig S8 and Table S1).

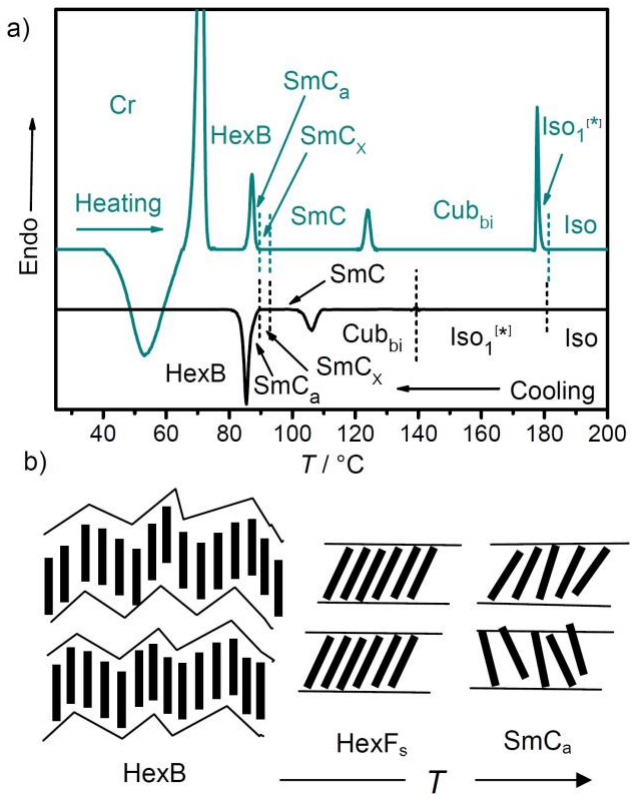

Figure 9. a) DSC heating and cooling traces (10 K min^{-1}) of compound **8** with the phase sequence HexB-SmC$_a$-SmC$_x$-SmC-Iso$_1^{[*]}$-Iso and b) sketch showing the HexB-HexF$_s$-SmC$_a$ transition of compound **7**.

The HexB low temperature phase is also found for the next homologue **8** below 86 °C. However, in this case, the phase sequence is a bit more complicated (Fig. 9a). On cooling the homeotropic aligned SmC$_s$ phase the birefringence at first decreases (Fig. 10d) and it becomes isotropic between 94 and 91 °C (Fig. 10c), then the texture becomes birefringent (Fig. 10b) and at the phase transition to the HexB phase at 86 °C ($\Delta H \sim 3$ kJ mol^{-1}) it becomes isotropic again (Fig. 10a).

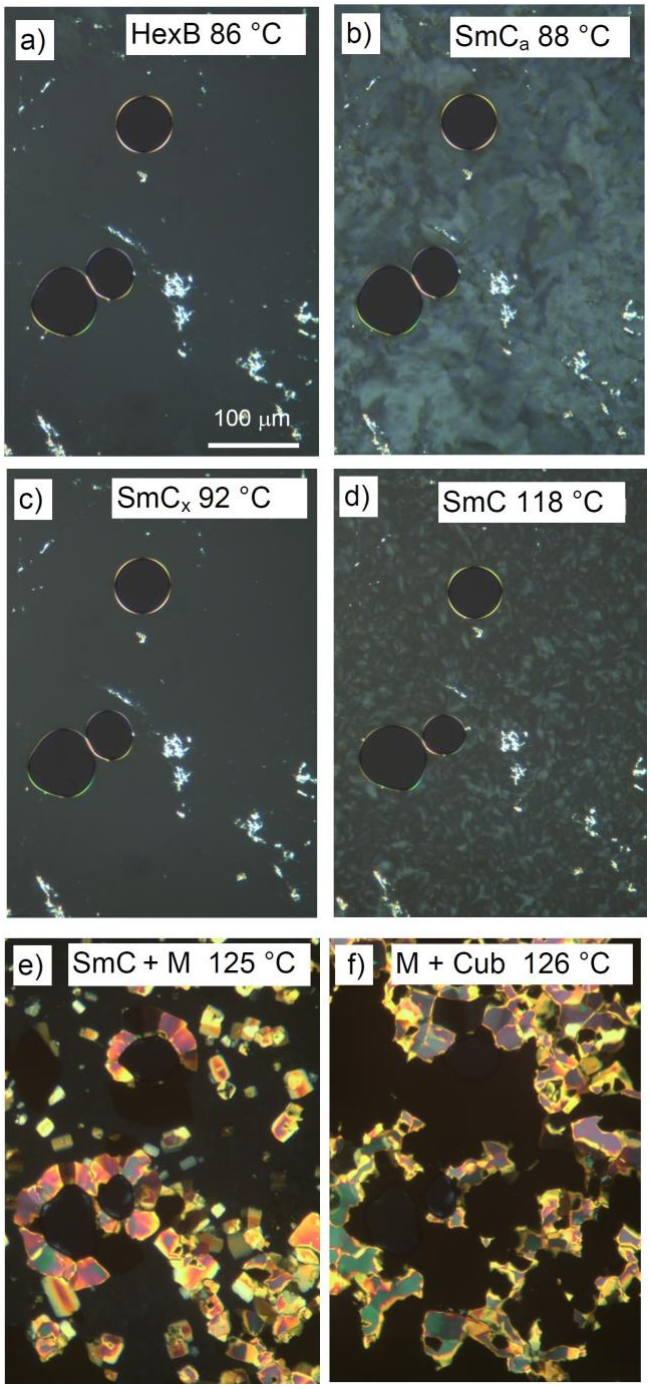

Figure 10. Textures of compound **8** as observed on heating (after cooling from the isotropic liquid state) in homeotropic alignment (between plain microscopy glass plates) in the designated phases at the given temperatures. In e) the majority of the dark area is the homeotropic SmC_a phase (the low birefringent Schlieren texture is invisible due to the shorter exposure time compared to d)) whereas in f) the dark areas represent the growing cubic phase.

In order to understand the structures of the two uniaxial smectic phases of compound **8**, and to check if for this compound the synclinic-anticlinic transition might be associated with formation of heliconical phases, as known for SmC* and SmCα* phases of chiral rod-like

molecules[70,79, 118] and SmC^{hel} phases of achiral bent molecules,[49,53] this compound was investigated by RSoXS at the carbon K-edge.[119,120] No resonant peak is observed in the unixial hexatic phase range below 87 °C, excluding a heliconical structure as origin of the optical uniaxiality and confirming the proposed non-tilted HexB structure. Upon heating, a resonant peak corresponding to twice the *d*-value of the non-resonant (01) layer scattering occurs in the temperature range between 87 and 91 °C (see Fig. 11c, Table S6 and Fig. S15), indicating a two-layer unit cell and thus an anticlinic SmC_a structure in the biaxial phase immediately following the HexB phase on heating (Table 2). Therefore, we attribute this temperature range to an anticlinic SmC_a phase. Above 91 °C the resonant peak is lost and only the non-resonant layer reflection can be observed, meaning that this smectic phase cannot be anticlinic. It also excludes a short pitch heliconical phase structure[49,52,53] as the origin of optical uniaxiality of this tilted smectic phase in the temperature range between 91 and 94 °C. Even the birefringent SmC phase, observed above 94 °C and up to the transition to the cubic phase, does not show a resonant scattering and therefore cannot be a SmC_a phase. This is in line with textural observations showing that the planar fan textures with dark extinctions becomes slightly birefringent above 94 °C (Fig. S5). This could be due to a developing synclinic tilt in the temperature range designated as SmC. A anticlinic to synclinic transition via a heliconical intermediate phase[49,52,53] could in principle also be possible. However, there is no RSoXS indication for any helical pitch in the length range covered by the used experimental setup (< 40 nm).[121,122,123] Therefore, this uniaxial phase range between 91 and 94 °C is tentatively designated as Sm_X.[124] The optical uniaxiality of the tilted smectic phase could be explained by a longer helix outside the range covered by the RSoXs experiments or by a randomization of the tilt correlation between the layers. Moreover, in the SmC_x range there is the coexistence of the non-resonant layer reflections of the SmC and SmC_a phases (red and blue dots in Fig. 11a), so that uniaxiality could also result from macroscopic tilt randomization due to the development of a synclinic+anticlinic microdomain structure in this temperature range.

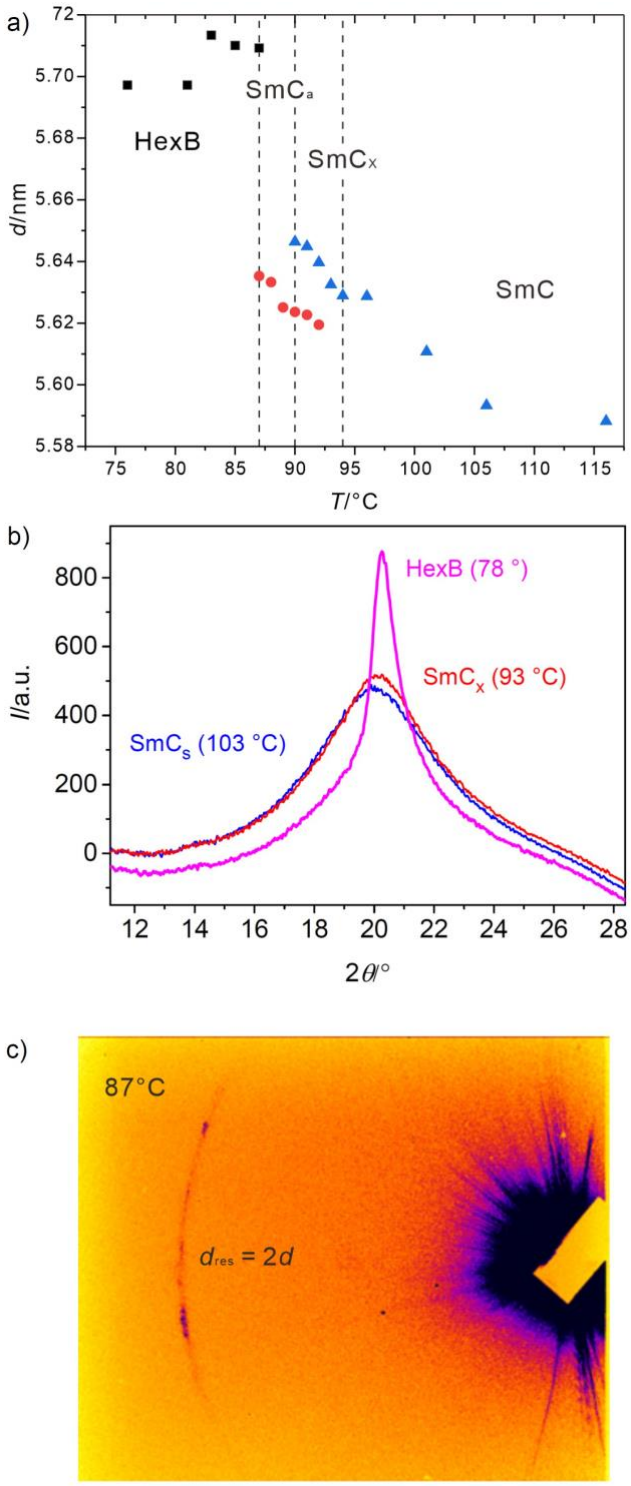

Figure 11. a) *d*-Spacings of the non-resonant (10) reflection observed on second heating in the lamellar phases of compound **8** (see Fig. S9 and Tab. S2, S3 for higher order reflections and WAXS data) and b) profiles of the wide angle scatterings; c) shows the resonant scattering (CCD image) at 87 °C on heating (for more details see Fig. S15 and Table S6).

Overall, in the smectic phase range there is an increasing tendency towards development of synclinic tilt with growing chain length, but only for compound **8** it obviously becomes

more dominating in the high temperature range of the SmC phase. However, even for this compound, at lower temperature there is still a tendency of the swallow-tailed molecules to assume an anticlinic tilt which we attribute to the contribution of the Y-shaped conformation (Fig. 4d). In this conformation the out-of-plane interlayer fluctuations are suppressed and hence the anticlinic tilt is favored. Because for compound **8** the tilt is relatively small, there appears to be no discrete synclinic-anticlinic transition, but instead this transition takes place in a disordered way by an intermediate loss of tilt correlation or a long pitch helical structure.

After transformation to the SmC_a phase, further cooling leads to the non-tilted HexB phase. However, for the next longer homologues **9-12** the hexatic phase becomes biaxial again (Fig. S6, S7, S10 and S11). This indicates a $HexI_s$-HexB-$HexI_s$ sequence with a re-entrance of synclinic tilt in the hexatic phases upon chain elongation. A possible model for the HexB phase, which explains this unexpected sequence, could be based on a modulated $HexI_s$ structure with a layer modulation by anticlinic defects in the form of closed contour loops, as proposed by Korlacki et al. (Fig. 9b).[125] Thus, the fundamental phase type is still $HexI_s$ which is retained for all compounds **8-12**, despite optical investigations indicate a $HexI_s$-HexB-$HexI_s$ sequence with a re-entrance of synclinic tilt upon chain elongation. For the long chain homologues **10** and **12** the non-modulated synclinic $HexI_s$ phase remains the only lamellar phase occurring below the Cub_{bi} phase (Figs. S11 and Table S5). Moreover, it appears that with growing chain length the $HexF_s$ phase range tightens and for compound **8** it is removed and completely replaced by the HexB phase.

3.1.5 Cubic and non-cubic 3D phases of compounds 7-12

An optically isotropic Cub_{bi} phase was observed for all compounds with chain length n = 7-12 as high temperature phase. The $1/d$ values appear in a ratio $\sqrt{3}:\sqrt{8}:\sqrt{14};\sqrt{16}$…etc., which can be indexed to a cubic lattice with $Ia3;\bar{d}$ symmetry and cubic lattice parameters a_{cub} = 10.0±0.4 nm (see Table S5). As shown in Fig. 1, the Cub_{bi} phase occurs at a chain length of $n \geq 7$ and replaces the SmA phase. For compounds **7-9** the SmC phase is retained below this Cub_{bi} phase, whereas for longer chain lengths (n = 10-12) only the $HexI_s$ phase is observed besides the dominating Cub_{bi} phase (see data of compound **9** in Fig. S6 and S9). Due to the hysteresis of the lamellar-Cub_{bi} transition some of the lamellar phases of the longer homologues can only be observed on heating.

The formation of these Cub_{bi} phase is the result of increasing interface curvature between the aromatic cores and the aliphatic chains, growing with the chain length n and temperature

(Fig. 1). In addition, increasing chain length *n* leads to a growing incompatibility of these chains with the aromatic cores. Thus, these chains become more likely to be expelled out of the aromatic layers into the layers of the 3,5-chains (transition c→b→a in Fig. 4), where they further increase the steric distortion of flat layers and support the development of saddle-splay curvature. As also shown in Fig. 12, the lateral distance between the two enantiomorphic nets in the $Ia3;\bar{d}$ phase (Fig. 13h), calculated according to $d_{net,cub} = \sqrt{3}(a_{cub}/4)$ is significantly shorter than the molecular length and this difference increases with the alkyl chain length *n*. This indicates a completely segregated organization of polyaromatic cores and alkyl chains (Fig. 4a) in the Cub_{bi} phases; the remaining difference between d_{net} and L_{mol} is due to additional chain folding, required to fill the space completely.

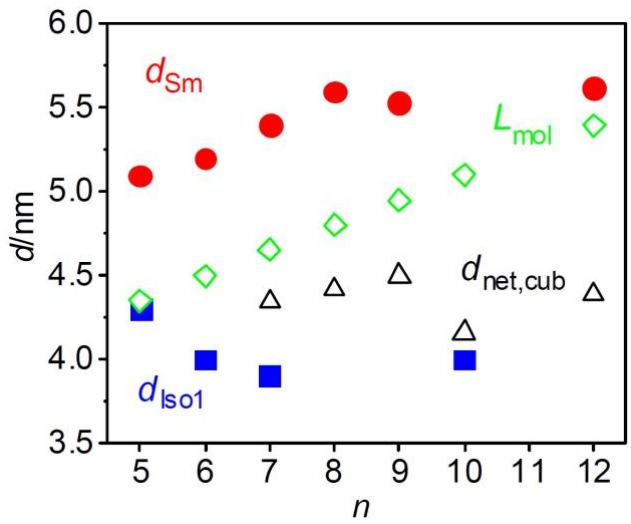

Figure 12. Development of the *d*-values of the layer reflection in the lamellar phase (d_{Sm}; **5**: SmA, **6-8**: SmC_a, **9**,**12**: $HexI_s$), position of the diffuse small angle scattering maximum in the $Iso_1/Iso_1^{[*]}$ phases (d_{Iso1}, 2K below the Iso-$Iso_1/Iso_1^{[*]}$ transition), network distance in the $Cub_{bi}/Ia3;\bar{d}$ phase ($d_{net,cub}$) and molecular length (L_{mol}) depending on chain length (*n*); for lattice parameters of the cubic phases, see Table S5.

Simultaneously with the transition from the SmC_a or SmC_s phase to the cubic phase on heating, highly birefringent areas with rectangular shape develop in the homeotropic samples of compounds **7** and **8**, respectively (M-phase, see Fig. 10e,f and Fig. S4). These highly birefringent domains have a high viscosity and rapidly disappear and transform into the cubic phase, indicating that this birefringent mesophase is metastable with respect to the cubic phase and presumably represents a distorted cubic lattice, probably with tetragonal or orthorhombic symmetry. This metastable M phase is absent for the higher homologues and thus is considered as another competing intermediate structure at the lamellar-Cub_{bi}

transition. Details of the structure of the $Cub_{bi}/Ia3;\bar{}d$ phases, representing two helical networks with opposite handedness (Fig. 13h) have been discussed previously.[23,69,119]

3.1.6 Percolated Iso_1 and $Iso_1^{[*]}$ phases of compounds 5-12

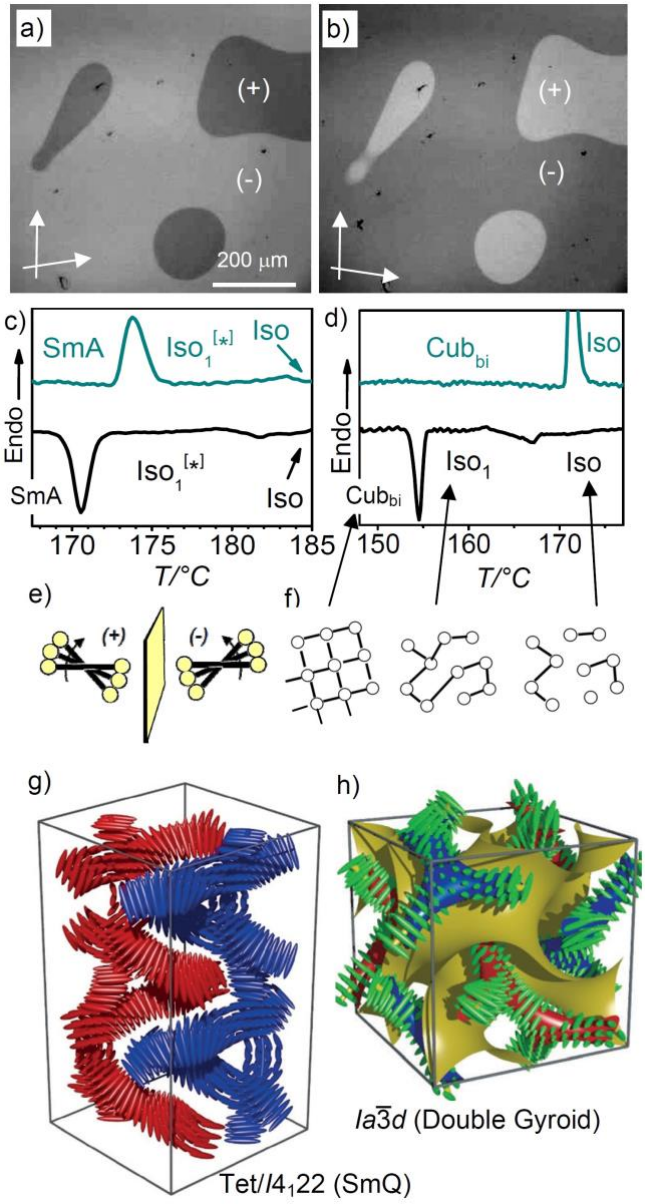

Figure 13. a, b) Chiral domains in the $Iso_1^{[*]}$ phase of compound **6** at T = 104 °C as observed by polarizing microscopy between slightly uncrossed polarizers; changing the twist between the polarizer from <90° to >90° leads to an inversion of the brightness of the domains, indicating the optical rotation in opposite directions (contrast enhanced); c, d) expanded sections of the DSC traces showing c) the Iso-$Iso_1^{[*]}$ transition of **6** on heating (top) and cooling (bottom, for complete curves, see Fig. S1) and d) the Iso-Iso_1 transition of compound **10**; e) shows the origin of the helical superstructure due to the clashing of the bulky end chains of the rod-like molecules (yellow dots) arranged with the molecular long axis perpendicular to the local network direction; f) illustrates the development of the networks by fusing short helical segments to clusters in the Iso range, followed by dynamic network formation in Iso_1, and with long range transmission of helicity in $Iso_1^{[*]}$, and finally the

establishment of the long range cubic lattice after further increase of the network connectivity in the Cub_{bi} phase; g) and h) show the helical structures in the g) SmQ phase (with uniform helix sense and four-way junctions) and h) $Ia3;\bar{d}$ phase (opposite helix sense in blue and red networks with three way junctions), representing the local structures in the chiral $Iso_1^{[*]}$ and the achiral Iso_1 phases, respectively; g, h) were reproduced with permission from refs. 37 and 23, respectively, by permission form Wiley-VCH.

The Iso-Cub transition on cooling is significantly delayed by 19-53 K, the difference decreasing with growing *n*. The Cub_{bi} phases of compounds **7-12** are not directly formed from the ordinary isotropic liquid (Iso), but there is a small region of a chiral ($Iso_1^{[*]}$) or achiral (Iso_1) liquid mesophase before the transition to the Cub_{bi} phase (Table 1, Fig. 13c,d and S1). For compounds **5-8** the mirror symmetry broken $Iso_1^{[*]}$ phase, characterized by fluid conglomerates of chiral domains with opposite handedness (see Fig. 13a-c),[12,21,22,61,69] occurs either between the achiral Iso phase and SmA (n = 5, 6) or between Iso and Cub_{bi} (n = 7, 8, see Table 1 and Fig. 1). The DSC traces of the long chain homologues **9-12** indicate a broad transition to an achiral Iso_1 phase occurring between the achiral Iso and $Cub_{bi}/Ia3;\bar{d}$ phases on cooling (Fig. 13d), whereas on heating a direct $Cub_{bi}/Ia3;\bar{d}$-Iso transition takes place. Hence, the achiral Iso_1 phase of compounds **9-12** is only monotropic. In the Iso_1 and $Iso_1^{[*]}$ ranges there are two diffuse XRD scatterings, one in the small and the other in the wide angle region of the XRD patterns. This is in line with the presence of only short range order, as typical for isotropic liquids with a locally ordered cluster structure (cybotaxis)[126,127] and for percolated liquids[128] often occurring besides frustrated LC phases (blue phases, Twist Grain Boundary phases, SmQ phases, etc.).[129130,131,132,133,134]

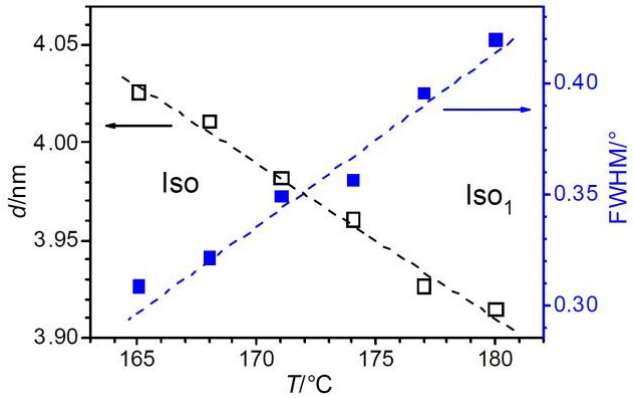

Figure 14. a) Development of *d*-values and line width (FWHM) of the small angle scattering maximum of compound **10** across the Iso-Iso_1 transition.

As shown in Fig. 14 for compound **10**, as example, the change of the line width of the XRD small angle scattering at the Iso-Iso_1 transition is continuous without any distinct jump, as

also found for the Iso-Iso$_1^{[*]}$-transitions.[21,25] The correlation length calculated with the Scherrer equation (assuming K = 1) is ~10 nm in the Iso phase at 180 °C and continuously grows to ~14 nm in the Iso$_1$ phase at 165 °C, corresponding to a bit more than just one cubic unit cell. The transition from the chiral Iso$_1^{[*]}$ phase to the achiral Iso$_1$ phase upon chain elongation could either be due to a decreasing network density, falling below the critical length for long range chirality transmission, or due to a change of the local structure. It is chiral, presumably SmQ-like (Fig. 13g),[37] for the chiral Iso$_1^{[*]}$ phase of compounds **5-8** and likely to be achiral (racemic) $Ia\bar{3}d$-like (Fig. 13h) for the achiral Iso$_1$ phase of the longer homologues **9-12**.[25,27]

3.2 Fluorinated compounds 6F and 6F$_2$

For compound **6** the influence of introduction of one or two fluorine atoms into the polyaromatic core at the monosubstituted peripheral benzene ring was investigated. Both compounds **6F** and **6F$_2$** (Scheme 1 and Table 1) show exclusively the Cub$_{bi}$/$Ia\bar{3}d$ phase (**6F**: a_{Cub} = 9.46 nm; **6F$_2$**: a_{Cub} = 9.35 nm) which is achiral and does not transform into a smectic phase nor crystallizes on cooling; crystallization is only observed on re-heating (see DSCs in Fig. S1g,h). Figure 15 shows the diffraction pattern and the reconstructed electron density map of the Cub$_{bi}$ phase of **6F**, as example, confirming the $Ia\bar{3}d$ lattice and the bicontinuous network structure (see Fig. S13 for XRD of **6F$_2$**). Compared with the non-fluorinated compound **6**, which only forms smectic LC phases and the Iso$_1^{[*]}$ phase, for both fluorinated compounds **6F** and **6F$_2$** the Iso$_1^{[*]}$ phases as well as the lamellar phases are completely removed. Core fluorination reduces the electron density of the π-system and thus increases the attractive core-core interactions, which obviously excludes the terminal alkyl chains from intercalation (Fig. 4c→b→a).[135,136,137,138] This is confirmed by the lateral distances between the networks, which are 4.10 nm (**6F**) and 4.05 nm (**6F$_2$**), respectively, being significantly smaller than the fully stretched molecular length (L_{mol} = 4.5 nm, Fig. 4a). This organization provides increased interface curvature despite of the larger diameter of the fluorinated aromatic cores (Fig. 4c→a). The thus increased interface curvature between aromatic and aliphatic domains favours the cubic phases.

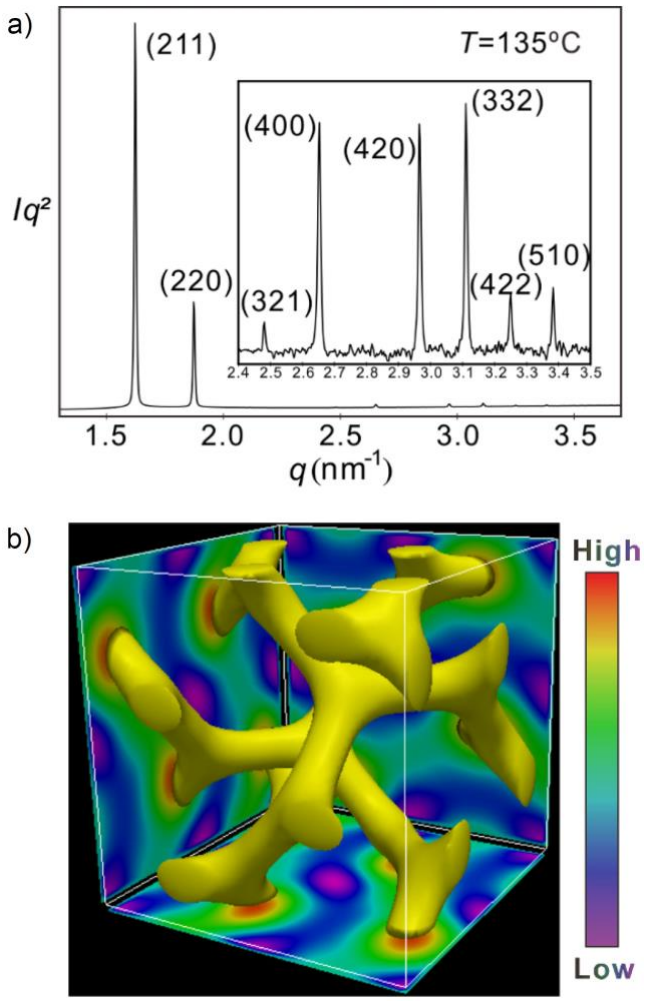

Figure 15. a) SAXS diffractogram of compound **6F** at 135 ºC, the experimental and calculated *d*-spacing of the observed SAXS reflection are given in Tab S4; for WAXS data, see Fig. S14; b) reconstructed 3D electron density map obtained from this powder pattern, showing the network structure of the $Ia3;\bar{}d$ phase; for electron density histogram, see Fig. S12; for XRD data of **6F**$_2$, see Figs. S13 and Table S5.

4. Summary and Conclusions

A series of achiral azobenzene-based tricatenar molecules with a 3,5-disubstitution pattern at one end is reported. This series of compounds provides a rich variety of distinct modes of LC self-assembly. It includes hexatic phases ($HexF_s$, $HexI_s$, HexB), a non-tilted SmA phase, synclinic and anticlinic tilted smectic C phases (SmC_s, SmC_a), a bicontinuous cubic phase with $Ia3;\bar{}d$ lattice, a non-cubic birefringent phase with 3D lattice and chiral ($Iso_1^{[*]}$) as well as achiral (Iso_1) isotropic liquid mesophases with local network structure. Especially notable are the broad regions of the rare SmC_a phases achieved with these achiral compounds, providing a new design concept for anticlinic smectics, eventually leading to practically important orthoconic LCs.[104] Moreover, the phase transitions from smectic to hexatic phases

is associated with a change of the layer correlation from anticlinic to synclinic on cooling, which is opposite to the usually observed SmC_s to SmC_a transitions. Obviously the alkyl chains in the 3,5-positions lead to a Y-shaped molecular conformation (Fig. 4d) which supports the anticlinic tilt. An increasing contribution of *trans*-conformers in the alkyl chains at lower temperature reduces the effects of chain disorder and supports the parallel alignment of the alkyl chain, thus leading to the development of a tuning fork like conformation (Fig. 4c), allowing improved out-of-plane inter-layer fluctuations and thus leading to the emergence of synclinic tilt correlation. Simultaneously, this conformation enables a denser packing, thus favouring the development of hexatic phases. This means that the anticlinic-synclinic and the smectic-hexatic transition are coupled.

Another remarkable feature of these compounds is the development of a helical twist in the chiral $Iso_1^{[*]}$ phase. These chirality synchronized isotropic liquid phases ($Iso_1^{[*]}$) occur for compounds with medium alkyl chain length (n = 5-8). Upon further chain elongation ($n \geq 9$) only achiral percolated Iso_1 phases can be observed (Fig. 1). Development of these $Iso_1/Iso_1^{[*]}$ phases is explained by dynamic network formation after crossing a critical connectivity of the helical aggregates (Fig. 13f), and if, in addition, a homogeneously chiral (e.g. SmQ-like, Fig. 13g) local network structure can develop in the $Iso_1^{[*]}$ phase. If the critical network density is not achieved or an achiral network structure (e.g. $Ia3;\bar{d}$, Fig. 13f) is preferred, then the percolated network liquid is achiral (Iso_1).

Finally the peripheral fluorination of the aromatic core unit was found to be a powerful tool for stabilization of bicontinuous cubic phases of polycatenar compounds. Though cubic phases are usually found only in relatively small temperature ranges, for the fluorinated compounds **6F** and **6F$_2$** wide ranges, even extended below ambient temperature, were observed. This effect of core fluorination is opposite to central core fluorination of other (symmetric) polycatenars which is known to give only smectic phases.[139] Functionality of the reported compounds is provided by the organization of the azobenzene units either in an anticlinic or helical fashion and the possibility of light-induced switching the molecular shape and phase type by *trans-cis* isomerization. This was recently demonstrated for chirality switching[67] and could lead to numerous potential applications as photo-tuneable optical and photonic materials.[140]

Acknowledgements

This work was supported by the Deutsche Forschungsgemeinschaft (Ts 39/24-2).

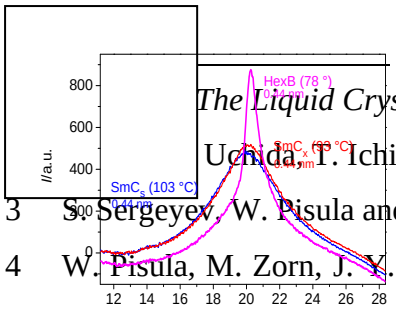

The Liquid Crystal Display Story, Springer Tokyo, 2014.

Uchida, T. Ichikawa and T Sakamoto, *Angew. Chem. Int. Ed.*, 2018, **57**, 4355.

3 S. Sergeyev, W. Pisula and Y. H. Geerts, *Chem. Soc. Rev.*, 2007, **36**, 1902.

4 W. Pisula, M. Zorn, J. Y. Chang, K. Müllen and R. Zentel, *Macromol. Rapid Commun.* 2009, **30**, 1179.

5 T. Kato, M. Yoshio, T. Ichikawa, B. Soberats, H. Ohno and M. Funahashi, *Nat. Rev. Mater.*, 2017, **2**, 17001.

6 C. Sinturel, F. S. Bates and M. A. Hillmyer, *ACS. Macro. Lett.*, 2015, **4**, 1044.

7 K. Nickmans and A. P. Schenning, *Adv. Mater.*, 2018, **30**, 1703713.

8 A. Lehmann, A. Scholte, M. Prehm, F. Liu, X.B. Zeng, G. Ungar and C. Tschierske, *Adv. Funct. Mater.*, 2018, **28**, 1804162.

9 C. Tschierske, *Angew. Chem. Int. Ed.*, 2013, **52**, 8828.

10 *Chirality in Liquid Crystals*, ed. H. S. Kitzerow and C. Bahr, Springer, New York, 2001.

11 I. Nishiyama, *Chem Rec.*, 2009, **9**, 340.

12 C. Tschierske, *Liq. Cryst.*, 2018, **45**, 2221.

13 J. W. Goodby, P. J. Collings, T. Kato, C. Tschierske, H. F. Gleeson, P. Raynes, eds., *Handbook of Liquid Crystals*, 2nd Ed., Wiley-VCH, Weinheim 2014.

14 R. A. Reddy and C. Tschierske, *J. Mater. Chem.*, 2006, **16**, 907.

15 A. Eremin and H. Takezoe, *Bent-shaped Liquid Crystals. Structures and Physical Properties; CRC Press, Taylor & Francis Group, Boca Raton, FL*, 2017.

16 J. Malthête, H. T. Nguyen and C. Destrade, *Liq. Cryst.*, 1993, **13**, 171.

17 a) H.-T. Nguyen, C. Destrade and J. Malthête, *Adv. Mater.*, 1997, **9**, 375; b) M. Gharbia, A. Gharbi, H. T. Nguyen and J. Malthête, *J. Curr. Opin. Colloid Interface Sci.*, 2002, **7**, 312.

18 a) D. Fazio, C. Mongin, B. Donnio, Y. Galerne, D. Guillon and D. W. Bruce, *J. Mater. Chem.*, 2001, **11**, 2852; b) D. W. Bruce, *Acc. Chem. Res.*, 2000, **33**, 831.

19 W. Weissflog in J. W. Goodby, P. J. Collings, T. Kato, C. Tschierske, H. F. Gleeson and P. Raynes, eds., *Handbook of Liquid Crystals*, 2nd Ed., Wiley-VCH, Weinheim 2014, **Vol. 5**, 89-174.

20 T. Yasuda, H. Ooi, J. Morita, Y. Akama, K. Minoura, M. Funahashi, T. Shimomura and T. Kato, *Adv. Funct. Mater.*, 2009, **19**, 411.

21 C. Dressel, T. Reppe, M. Prehm, M. Brautzsch and C. Tschierske, *Nat. Chem.*, 2014, **6**, 971.

22 C. Tschierske and G. Ungar, *ChemPhysChem.*, 2016,**19**, 9.

23 C. Dressel, F. Liu, M. Prehm, X-B Zeng, G. Ungar and C. Tschierske, *Angew. Chem. Int. Ed.*, 2014, **53**, 13115.

24 T. Reppe, C. Dressel, S. Poppe, C. Tschierske, *Chem. Commun.* **2020**, *56*, 711

25 T. Reppe, S. Poppe, X. Cai, Y. Cao, F. Liu, C. Tschierske, *Chem. Sci*. **2020**, *11*, 5902.

26 C. Dressel, T. Reppe, S. Poppe, M. Prehm, H. Lu, X. Zeng, G. Ungar, C. Tschierske, *Adv.Funct.Mater.* **2020**, DOI: 10.1002/adfm.202004353.

27 T. Reppe, S. Poppe, C. Tschierske, *Chem Eur. J.* **2020**, *26*, DOI:10.1002/chem.20200286.

28 J. Kain, S. Diele, G. Pelzl, C. Lischka and W. Weissflog, *Liq. Cryst.*, 2000, **27**, 11.

29 A.-M. Levelut, B. Donnio and D. W. Bruce, *Liq. Cryst.*, 1997, **22**, 753.

30 a) T. Yamamoto, I. Nishiyama, M. Yoneya and H. Yokoyama, *J. Phys. Chem. B*, 2009, **113**, 11564; b) M. Yoneya, *The Chemical Record*, 2011, **11**, 66.

31 X. Zeng, G. Ungar and M. Impéror-Clerc, *Nat. Mater.* 2005**, 4**, 562.

32 X. B. Zeng, G. Ungar, *J. Mater. Chem. C* **2020**, *8*, 5389.

33 A. M. Levelut, C. Germain, P. Keller, L. Liebert and J. Billard, *J. Phys.*, 1983, **44**, 623.

34 A. M. Levelut, E. Hallouin, D. Bennemann, G. Heppke and D. Loetzsch, *J. Phys. II*, 1997, **7**, 981.

35 B. Pansu, Y. Nastishin, M. Imperor-Clerc, M. Veber and H. T. Nguyen, *Eur. Phys. J. E*, 2004, **15**, 225.

36 M. Vogrin, N. Vaupotič, M. M. Wojcik, J. Mieczkowski, K. Madrak, D. Pociecha and E. Gorecka, *Phys.Chem.Chem.Phys.*, 2014, **16**, 16067.

37 H. Lu, X. Zeng, G. Ungar, C. Dressel and C. Tschierske, *Angew. Chem. Int. Ed.*, 2018, **57**, 2835.

38 H. Takezoe, Spontaneous Achiral Symmetry Breaking in Liquid Crystalline Phases. In Liquid Crystals; Tschierske, C., Ed.; *Topics in Current Chemistry; Springer: Berlin*, 2011, **Vol. 318**, pp 303−330.

39 V. Borshch, Y.-K. Kim, J. Xiang, M. Gao, A. Ja´kli, V. P. Panov, J. K. Vij, C. T. Imrie, M. G. Tamba, G. H. Mehl and O. D. Lavrentovich, *Nat. Commun.*, 2013, **4**, 2635.

40 I. Dozov, *Europhys. Lett.*, 2001, **56**, 247.

41 V. P. Panov, J. K. Vij and G. H. Mehl, *Liq. Cryst.*, 2017, **44**, 147.

42 R. J. Mandle, J. W. Goodby, *Soft Matter*, 2016, **12**, 1436.

43 R. J. Mandle, *Chem. Rec.*, 2018, **18**, 1.

44 M. Salamończyk, N. Vaupotic, D. Pociecha, C. Wang, C. Zhu and E. Gorecka, *Soft Matter*, 2017, **13**, 6694.

45 D. Chen, J. H. Porada J. B. Hooper, A. Klittnick, Y. Shen, M. R. Tuchband, E. Korblova, D. Bedrov, D. M. Walba, M. A. Glaser, J. E. Maclennan and N. A. Clark, *Proc. Natl Acad. Sci. USA*, 2013, **110**, 15931.

46 C. Zhu, M. R. Tuchband, A. Young, M. Shuai, A. Scarbrough, D. M. Walba, J. E. Maclennan, C. Wang, A. Hexemer and Noel A. Clark, *Phys Rev Lett.*, 2016, **116**, 147803.

47 J. P. Abberley, S. M. Jansze, R. Walker, D. A. Paterson, P. A. Henderson, A. T. M. Marcelis, J. M. D. Storey and C. T. Imrie, *Liq. Cryst.*, 2017, **44**, 68.

48 W. D. Stevenson, Z. Ahmed, X. B. Zeng, C. Welch, G. Ungar G. H. Mehl, *Phys.Chem.Chem.Phys.*, 2017, **19**, 13449.

49 S. P. Sreenilayam, Y. P. Panarin, J. K. Vij, V. P. Panov, A. Lehmann, M. Poppe, M. Prehm and C. Tschierske, *Nat. Commun.*, 2016, **7**, 11369.

50 A. Lehmann, M. Alaasar, M. Poppe, S. Poppe, M. Prehm, M. Nagaraj, S. P. Sreenilayam, Y. P. Panarin, J. K. Vij and Carsten Tschierske, *Chem. Eur. J.* 2020, **26**, 4714.

51 a) Y. P. Panarin, M. Nagaraj, S. Sreenilayam, J. K. Vij, A. Lehmann and C. Tschierske, *Phys. Rev. Lett.*, 2011, **107**, 247801; b) M. Alaasar, M. Prehm, M. Poppe, M. Nagaraj, J. K. Vij and C. Tschierske, *Soft Matter*, 2014, **10**, 5003; c) S. P. Sreenilayam, Yu. P. Panarin, J. K. Vij, A. Lehmann, M. Poppe and C. Tschierske, *Phys. Rev. Mater.*, 2017, **1**, 035604.

52 A. A. S. Green, M. R. Tuchband, R. Shao, Y. Shen, R. Visvanathan, A. E. Duncan, A. Lehmann, C. Tschierske, E. D. Carlson, E. Guzman, M. Kolber, D. M. Walba, C. S. Park, M. A. Glaser, J. E. Maclennan and N. A Clark, *Phys. Rev. Lett.*, 2019, **122**, 107801.

53 a) J. P. Abberley, R. Killah, R. Walker, J. M. D. Storey, C. T. Imrie, M. Salamonczyk, C. Zhu, E. Gorecka and D. Pociecha, *Nat. Commun.*, 2018, **9**, 228; b) M. Salamończyk, N. Vaupotič, D. Pociecha, R. Walker, J. M.D. Storey, C. T. Imrie, C. Wang, C. Zhu and E. Gorecka, *Nat. Commun.*, 2019, **10**,1922.

54 G. Dantlgraber, A. Eremin, S. Diele, A. Hauser, H. Kresse, G. Pelzl and C. Tschierske. *Angew. Chem. Int. Ed.*, 2002, **41**, 2408.

55 L. E. Hough, M. Spannuth, M. Nakata, D. A. Coleman, C. D. Jones, G. Dantlgraber, C. Tschierske, J. Watanabe, E. Körblova, D. M. Walba, J. E. Maclennan, M. A. Glaser and N. A. Clark, *Science*, 2009, **325**, 452.

56 K. V. Le, H. Takezoe and F. Araoka, *Adv. Mater.*, 2017, **29**, 1602737.

57 L. E. Hough, H. T. Jung, D. Kruerke, M. S. Heberling, M. Nakata, C. D. Jones, D. Chen, D. R. Link, J. Zasadzinski, G. Heppke, J. P. Rabe, W. Stocker, E. Korblova, D. M. Walba, M. A. Glaser and N. A. Clark, *Science*, 2009, **325**, 456.

58 S. Shadpour, A. Nemati, N. J. Boyd, L. Li, M. E. Prévôt, S. L. Wakerlin, J. P. Vanegas, M. Salamończyk, de E. Hegmann, C. Zhu, M. R. Wilson, A. I. Jákli and T. Hegmann, *Mater. Horiz.*, 2019, **6**, 959.

59 a) M. Alaasar, M. Prehm and C. Tschierske, *Chem. – Eur. J.*, 2016, **22**, 6583; b) M. Alaasar, M. Prehm and C. Tschierske, *RSC Adv.*, 2016, **6**, 82890; c) M. Alaasar, M. Prehm, M. Brautzsch and C. Tschierske, *J. Mater. Chem. C*, 2014, **28**, 5487; d) M. Alaasar, M. Prehm, M. Brautzsch and C. Tschierske, *Soft Matter*, 2014, **10**, 7285; e) M. Alaasar, M. Prehm and C Tschierske, *Chem. Commun.*, 2013, **49**, 11062; f) M. Kohout, M. Alaasar, A. Poryvai, V. Novotná, S. Poppe, C. Tschierske and J. Svoboda, *RSC Adv.*, 2017, **7**, 35805.

60 C. Dressel, W. Weissflog and C. Tschierske, *Chem. Commun.*, 2015, **51**, 15850.

61 C. Tschierske, C. Dressel, *Symmetry, 2020*, **12**, 1098; doi:10.3390/sym12071098.

62 H. M. D. Bandarab and S. C. Burdette, *Chem. Soc. Rev.*, 2012, **41**, 1809.

63 a) H. K. Bisoyi and Q. Li, *Chem. Rev.*, 2016, **116**, 15089; b) M. Alaasar, *Liq. Cryst.*, 2016, **43**, 2208.

64 a) X. Peng, H. Gao, Y. Xiao, H. Cheng, F. Huang and X. Cheng, *New J. Chem.*, 2017, **41**, 2004; b) M. Alaasar, S. Poppe and C. Tschierske, *J. Mol. liq.* **2019**, *277*, 233.

65 H. Chen, R. Zhang, H. Gao, H. Cheng, H. Fang and X. Cheng, *Dyes and Pigments*, 2018, **149**, 512.

66 N. G. Nagaveni, M. Gupta, A. Roy and V. Prasad, Veena, *J. Mater. Chem.*, 2010, **20**, 9089.

67 M. Alaasar, M. Prehm, Y. Cao, F. Liu and C. Tschierske, *Angew. Chem. Int. Ed.*, 2016, **55**, 320.

68 M. Alaasar, S. Poppe, Q. Dong, F. Liu and C. Tschierske, *Chem. Commun.*, 2016, **52**, 13869.

69 M. Alaasar, S. Poppe, Q. Dong, F. Liu and C. Tschierske, *Angew. Chem. Int. Ed.*, 2017, **56**, 10801.

70 H. Takezoe, E. Gorecka and M. Čepič, *Rev. Mod. Phys.*, 2010, 82, 897.

71 R. Pratibha, N. V. Madhusudana and B. K. Sadashiva, *EPL*, 2007, **80**, 46001.

72 R. Pratibha, N. V. Madhusudana and B. K. Sadashiva, *Science*, 2000, **288**, 2184.

73 T. Hegmann, J. Kain, S. Diele, G. Pelzl, and C. Tschierske, *Angew. Chem. Int. Ed.*, 2001, **40**, 887.

74 V. Yelamaggad, I. S. Shashikala, V. P. Tamilenthi, D. S. S. Rao, G. G. Nair and S. K. Prasad, *J. Mater. Chem.*, 2008, **18**, 2096.

75 B. K. Sadashiva, R. A. Reddy, R. Pratibha and N. V. Madhusudana, *Chem. Commun.*, 2001, **2140**.

76 K. Kishikawa, T. Inoue, Y. Sasaki, S. Aikyo, M. Takahashi and S. Kohmoto, *Soft Matter*, 2011, **7**, 7532.

77 J. Lagerwall and F. Giesselmann, *ChemPhysChem*, 2006, **7**, 20.

78 M. A. Glaser and N. A. Clark, *Phy. Rev. E*, 2002, **66**, 021711.

79 T. Matsumoto, A. Fukuda, M. Johno, Y. Motoyama, T. Yui, S.-S. Seomun and M. Yamashita, *J. Mater. Chem.*, 1999, **9**, 2051.

80 A. Yamaguchi, A. Yoshizawa, I. Nishiyama, J. Yamamoto and H. Yokoyama, *Mol. Cryst. Liq. Cryst.*, 2005, **439**, 85[1951].

81 H. J. Coles, S. Meyer, P. Lehmann, R. Deschenaux and I. Jauslin, *J. Mater. Chem.*, 1999, **9**, 1085.

82 D. Guillon, M. A. Osipov, S. Mery, M. Siffert, J.-F. Nicoud, C. Bourgogne and P. Sebastiao, *J. Mater. Chem.*, 2001, **11**, 2700.

83 G. Dantlgraber, S. Diele and C. Tschierske, *Chem. Commun.*, 2002, 2768.

84 N. Olsson, I. Dahl, B. Helgee and L. Komitov, *Liq. Cryst.*, 2004, **31**, 1555.

85 K. Kishikawa, N. Muramatsu, S. Kohmoto, K. Yamaguchi and M. Yamamoto, *Chem. Mater.*, 2003, **15**, 3443.

86 I. Nishiyama and J. W. Goodby, *J. Mater. Chem.*, 1992, **2**, 1015.

87 Y. Ouchi, Y. Yoshioka, H. Ishii, K. Seki, M. Kitamura, R. Noyori, Y. Takanishib and I. Nishiyama, *J. Mater. Chem.*, 1995, **5**, 2297.

88 J. Thisayukta and E. T. Samulski, *J. Mater. Chem.*, 2004, **14**, 1554.

89 a) S.-L. Wu and F.-D. Chen, *Liq. Cryst.*, 2003, **30**, 991–995; b) S.-L. Wu and F.-D. Chen, *Liq. Cryst.*, 2004, **31**, 607.

90 W. Drzewińsk, R. Dabrowski, K. Czupryński, J. Przedmojski and M. Neubert, *Ferroelectrics*, 1998, **212**, 281.

91 K.-T. Kang, S. K. Lee, C. W. Park, S. H. Cho, J. G. Lee, S.-K. Choi and Y. B. Kim, *Bull. Korean Chem. Soc.*, 2006, **27**, 1364.

92 I. Nishiyama, T. Yamamoto, J. Yamamoto, J. W. Goodbyb and H. Yokoyama, *J. Mater. Chem.*, 2003, **13**, 1868.

93 S. J. Cowling, A. W. Hall and J. W. Goodby, *Liq. Cryst.*, 2005, **32**, 1483.

94 H. T. Nguyen, J. C. Rouillon, A. Babeau, J. P. Marcerou, G. Sigaud, M. Cotrait and H. Allouchi, *Liq. Cryst.*, 1999, **26**, 1007.

95 R. Dabrowski, *Ferrofetlrics*, 2000, **243**, 1.

96 S.-L. Wu and C.-Y. Lin, *Liq. Cryst.*, 2005, **32**, 663.

97 The reason for the dominance of synclinic SmC_s phases in the polycatenar case might be that usually the 3,4-disubstitution or 3,4,5-trisubstitution pattern with a side-by-side organization of the alkyl chains were used and this appears to support synclinic SmC_s phase formation by parallel chain alignment.

98 F. C. Yu and L. J. Yu, *Chem Mater.*, 2006, **18**, 5410.

99 F. C. Yu and L. J. Yu, *Liq. Cryst.*, 2008, **35**, 799.

100 E. Enz, S. Findeisen-Tandel, R. Dabrowski, F. Giesselmann, W. Weissflog, U. Baumeister and J. Lagerwall, *J. Mater. Chem.*, 2009, **19**, 2950.

101 A. Chakraborty, B. Das, M. K. Das, S. Findeisen-Tandel, M.-G. Tamba, U. Baumeister, H. Kresse and W. Weissflog, *Liq. Cryst.*, 2011, **38**, 1085.

102 P. Sathyanarayana, S. Radhika, B. K. Sadashivab and S. Dhara, *Soft Matter*, 2012, **8**, 2322.

103 M. Alaasar, S. Poppe, C. Kerzig, C. Klopp, A. Eremin and C. Tschierske, *J. Mater. Chem. C*, 2017, **5**, 8454.

104 S. T. Lagerwall, A. Dahlgren, P. Jägemalm, P. Rudquist, K. D'havé, H. Pauwels, R. Dabrowski and W. Drzewinski, *Adv. Funct. Mater.*, 2001, **11**, 87.

105 M. Neundorf, Dissertation, Martin-Luther University Halle, 19XX. P. 56-59.

106 G. Albertini, S. Melone, G. Poeti, F. Rustichelli and G. Torquati, *Mol. Cryst. Liq. Cryst.*, 1984, **104:1-2**, 121.

107 G. W. Gray, J. W and G. Goodby, *Smectic Liquid Crystals, Leonard Hill and Glasgow*, 1984.

108 J. M. Seddon, Chapter 3, Structural Studies of Liquid Crystals by X-ray Diffraction, Handbook of Liquid Crystals, D. Demus, J. Goodby, G. W. Gray, H-W. Spiess and V. Vill, wiley-VCH, Weinheim, 1998, p. 635-679.

109 J. J. Benattar, F. Moussa, M. Lambert and C. Germain. *Journal de Physique Lettres*, 1981, **42**, 67.

110 P. A. C. Gane, A. J. Leadbetter, J. J. Benattar, F. Moussa and M. Lambert, *Phys. Rev. A*, 1981, **24**, 2694.

111 S. Shibahara, J. Yamamoto, Y. Takanishi, K. Ishikawa, H. Yokoyama and H. Takezoe, *Phys. Rev. E*, 2002, **65**, 030702(R).

112 Y. Takanishi, K. Miyachi, S. Yoshida, B. Jin, H. Yin, K. Ishikawa, H. Takezoe and A. Fukuda, *J. Mater. Chem.*, 1998, **8**, 1133.

113 M. Neundorf, Y. Takanishi, A. Fukuda, S. Saito, K. Murashiro, T. lnukai and D. Demus, *J. Mater. Chem.*, 1995, **5**, 2221.

114 I. Nishiyama, J. Yamamoto, J. W. Goodbyb and H. Yokoyama, *J. Mater. Chem.*, 2003, **13**, 2429.

115 S. Kundu, T. Ray, S. K. Roy and R. Dabrowski, *Liq. Cryst.*, 2004, **31**, 119.

116 F. Beaubois, V. Faye, J. P. Marcerou, H. T. Nguyen and J. C. Rouillon, *Liq. Cryst.*, 1999, **26**, 1351.

117 Because the SmC_a phase is formed from a cubic phase no specific textures can be observed.

118 M. Cepic, *ChemPhysChem* 2014, **15**, 1297.

119 Y. Cao, M. Alaasar, A. Nallapaneni, M. Salamończyk, P. Marinko, E. Gorecka, C. Tschierske, F. Liu, N. Vaupotič, and C. Zhu, *Phys. Rev. Lett.*, 2020, **125**, 027801.

120 V. Lewandowski, N. Vaupotic, D. Pociecha, E. Gorecka, L. M. Liz-Marzan, *Adv. Mater.* 2020, 1905591; Y. Cao, C. Feng, A. Jakli, C. Zhu, F. Liu, Giant, 2020, 100018, https://doi.org/10.1016/j.giant.2020.100018

121 A.-M. Levelut, B. Pansu, *Phys. Rev. E.*, 1999, **60**, 6803.

122 P. Mach, R. Pindak, A.-M. Levelut, P. Barois, H. T. Nguyen, C. C. Huang, and L. Furenlid, *Phys. Rev. Lett.*, 1998, **81**, 1015.

123 C. C. Huang, S. Wang, L. Pan, Z. Q. Liu, B. K. McCoy, Y. Sasaki, K. Ema, P. Barois, and R. Pindak, *Liq. Crys. Rev.*, 2015, **3**, 58.

124 A long pitch helicanical structure with a pitch > 40 nm (outside the range covered by the RSoXS set-up) and smaller than the visible wave length range cannot be excluded for the

SmC_x and the SmC_s ranges with zero or low birefringence of the homeotropic samples, respectively.

125 A. R. Korlacki, A. Fukuda and J. K. Vij, *EPL*, 2007, **77**, 36004.

126 a) C. Keith, A. Lehmann, U. Baumeister, M. Prehm and C. Tschierske, *Soft Matter*, 2010, **6**, 1704; b) M. Alaasar, M. Prehm and C. Tschierske, *Liq. Cryst.*, 2014, **41**,126; c) M. Alaasar, S. Poppe and C. Tschierske, *Liq. Cryst.*, 2017, **44**, 729.

127 O. Francescangeli, F. Vita and E. T. Samulski, *Soft Matter*, 2014, **10**, 7685.

128 Y. Zhuang and P. Charbonneau, *J. Phys. Chem. B*, 2016, **120**, 7775.

129 S. Kutsumizu, *Isr. J. Chem.*, 2012, **52**, 844.

130 J.P. Marcerou, R. Farhi, J.C. Rouillon and H.T. Nguyen, *Eur. Phys. J. E*, 2000, **3**, 29.

131 H.T. Nguyen, N. Ismaili, N. Isaert and M.F. Achard, *J. Mater. Chem.*, 2004, **14**, 2060.

132 J. W. Goodby, D. A. Dunmur and J. P. Collings, *Liq. Cryst.* 1995, **19**, 703.

133 M. Jasinski, D. Pociecha, H. Monobe, J. Szczytko and P. Kaszynski, *J. Am. Chem. Soc.*, 2014, **136**, 14658.

134 M. Manai, A. Gharbi, J. P. Marcerou, H. T. Nguyen and J. C. Rouillon, *Physica B*, 2005, **368**, 168.

135 C. A. Hunter and J. K. M. Sanders, *J. Am. Chem. Soc.*, 1990, **112**, 5525.

136 C. A. Hunter, K. R. Lawson, J. Perkins and C. J. Urch, *J. Chem. Soc., Perkin Trans.* 2001, **2**, 651.

137 S. E. Wheeler and J. W. G. Bloom, *J. Phys. Chem. A*, 2014, **118**, 6133.

138 K. Kishikawa, *Isr. J. Chem.*, 2012, **52**, 800.

139 A. I. Smirnova, B. Heinrich, B. Donnio and D. W. Bruce, *RSC Adv.*, 2015, **5**, 75149.

140 a) Q. Li (Ed.) *Photoactive Functional Soft Materials: Preparation, Properties, and Applications*, Wiley-VCH, Weinheim, Germany **2019**; b) H. K. Bisoyi, T. J. Bunning, and Q. Li, *Adv. Mater.*, 2018, 1706512.